Neoplasia 53 (2024) 101005

Contents lists available at ScienceDirect

Neoplasia

journal homepage: www.elsevier.com/locate/neo

Original Research

Enhanced $Apc^{Min/+}$ adenoma formation after epithelial CUL4B deletion by recruitment of myeloid-derived suppressor cells

Beibei Guo [a,b], Yawen Zheng [b,e], Yujia Fan [a,b], Yang Yang [a,b], Yuxing Wang [b], Liping Qin [b], Yachun An [a,b], Xiaoran Xu [a,b], Xiyu Zhang [b], Gongping Sun [c], Hao Dou [b], Changshun Shao [d], Yaoqin Gong [b], Baichun Jiang [b,*], Huili Hu [a,b,*]

[a] The Key Laboratory of Experimental Teratology, Ministry of Education, Department of Systems Biomedicine, School of Basic Medical Sciences, Shandong University, Jinan, China
[b] The Key Laboratory of Experimental Teratology, Ministry of Education, Department of Medical Genetics, School of Basic Medical Sciences, Shandong University, Jinan, China
[c] The Key Laboratory of Experimental Teratology, Ministry of Education and Department of Histoembryology, Shandong University Cheeloo Medical College, Shandong University School of Medicine, Jinan, China
[d] The First Affiliated Hospital of Soochow University and State Key Laboratory of Radiation Medicine and Protection, Institutes for Translational Medicine, Soochow University, Suzhou, China
[e] Department of Obstetrics & Gynecology, Qilu Hospital of Shandong University, Jinan, China

ARTICLE INFO

Keywords:
Adenomatous polyposis coli (APC)
Colorectal cancer (CRC)
Cullin 4B (CUL4B)
Myeloid-derived suppressor cells (MDSCs)
Tumor microenvironment (TME)

ABSTRACT

Colorectal cancer (CRC) stands as a prevalent malignancy globally. A pivotal event in CRC pathogenesis involves the loss-of-function mutation in the *APC* gene, leading to the formation of benign polyps. Despite the well-established role of *APC*, the contribution of CUL4B to CRC initiation in the pre-tumorous stage remains poorly understood. In this investigation, we generated a murine model by crossing $Apc^{Min/+}$ mice with $Cul4b^{\Delta IEC}$ mice to achieve specific deletion of *Cul4b* in the gut epithelium against an $Apc^{Min/+}$ background. By employing histological methods, RNA-sequencing (RNA-seq), and flow cytometry, we assessed alterations and characterized the immune microenvironment. Our results unveiled that CUL4B deficiency in gut epithelium expedited $Apc^{Min/+}$ adenoma formation. Notably, CUL4B in adenomas restrained the accumulation of tumor-infiltrating myeloid-derived suppressor cells (MDSCs). *In vivo* inhibition of MDSCs significantly delayed the growth of CUL4B deleted $Apc^{Min/+}$ adenomas. Furthermore, the addition of MDSCs to *in vitro* cultured $Apc^{Min/+}$; $Cul4b^{\Delta IEC}$ adenoma organoids mitigated their alterations. Mechanistically, CUL4B directly interacted with the promoter of *Csf3*, the gene encoding granulocyte-colony stimulating factor (G-CSF) by coordinating with PRC2. Inhibiting CUL4B epigenetically activated the expression of G-CSF, promoting the recruitment of MDSCs. These findings offer novel insights into the tumor suppressor-like roles of CUL4B in regulating $Apc^{Min/+}$ adenomas, suggesting a potential therapeutic strategy for CRC initiation and progression in the context of activated Wnt signaling.

Introduction

Cullin 4B (CUL4B), a scaffold protein of the E3 ubiquitin ligase complex, plays a role in various physiological processes, including protein degradation and transcriptional repression through histone ubiquitylation [1,2]. CUL4B has been reported to be overexpressed in multiple tumors, including colorectal cancer (CRC), while its impact on carcinogenesis is not fully elucidated. Previous studies have demonstrated that *CUL4B* knockdown in tumor cell lines suppresses proliferation, migration, invasion, sphere formation, and subcutaneous

Abbreviations: APC, Adenomatous polyposis coli; CRC, Colorectal cancer; CUL4B, Cullin 4B; MDSCs, Myeloid-derived suppressor cells; TME, Tumor microenvironment; G-CSF, Granulocyte-colony stimulating factor; ISCs, Intestinal stem cells; EMT, Epithelial-mesenchymal transition; LOH, Loss of heterozygosity; COAD, Colorectal adenocarcinoma; LUAD, Lung adenocarcinoma; PRAD, Prostate adenocarcinoma; TCGA, The Cancer Genome Atlas; RNA-seq, RNA sequencing; DEGs, Differentially expressed genes; PRC2, Polycomb repressive complex 2; TTS, Transcription start site; TDSFs, Tumor-derived suppressor factors; SEM, Standard error of the mean.

* Corresponding authors.
E-mail addresses: jiangbaichun@sdu.edu.cn (B. Jiang), huhuili@sdu.edu.cn (H. Hu).

https://doi.org/10.1016/j.neo.2024.101005
Received 4 December 2023; Received in revised form 10 April 2024; Accepted 10 May 2024

tumorigenesis [3–8]. Interestingly, recent findings indicate a reverse effect of CUL4B in immune cells, revealing that hematopoietic or myeloid cell-specific deletion of CUL4B accelerates carcinogenesis [9, 10]. It is evident that the role of CUL4B on tumors remains not fully deciphered.

Colorectal cancer (CRC) stands as a prevalent and lethal malignancy, ranking third in incidence and second in mortality globally [11]. The stepwise development of CRC is driven by the sequential acquisition of specific genetic changes [12]. The most common event in CRC, occurring in 80 % of cases, is the *APC* loss-of-function mutation, leading to aberrant activation of the Wnt/β-catenin signaling pathway and formation of benign polyps [13,14]. Nevertheless, inhibition of identified markers or pathways is often accompanied by resistance or non-effect [15], causing that better understanding of CRC onset and improved knowledge of early screen indicator urgent attention.

Overall, CUL4B facilitates malignant behaviour and accelerates CRC progression [16]. Mechanistically, epithelial-mesenchymal transition (EMT) and Wnt/β-catenin signaling pathway are animated by CUL4B to strengthen drug resistance [17] and enhance cell proliferation [18], respectively. Moreover, CUL4B represses miR34a to maintain cancer stemness [3], conversely, CUL4B can be inhibited by miR431 to reduce migration and invasion ability in CRC [19]. Notably, most of the reported results used malignant CRC cell lines like HCT116, resulting in the neglect of the adenomatousgenesis of CRC. Besides, the reverse effect that specific deletion of CUL4B in hematopoietic or myeloid cells promotes carcinogenesis is demonstrated. However, the precise role of CUL4B in the spontaneous initiation of adenomas at the pre-tumor stage and tumor growth in CRC remains unknown.

In this study, we sought to address this knowledge gap by deleting the *Cul4b* gene in the gut epithelium of $Apc^{Min/+}$ mice, a preclinical model of inherited CRC. Our findings revealed that CUL4B serves as a limiting factor in the progression of adenomatous polyposis. Deletion of *Cul4b* in gut epithelium altered the tumor microenvironment (TME), specifically by enhancing the accumulation of myeloid-derived suppressor cells (MDSCs). Blocking the MDSCs rescued the increased $Apc^{Min/+}$ adenoma formation. Mechanistically, the accelerated onset of $Apc^{Min/+}$ adenomatousgenesis due to CUL4B loss was attributed to its role in transcriptional repression of *Csf3* in tumor cells. Together, our results unveil a novel mechanism, shedding light on the previously unknown function of CUL4B in promoting $Apc^{Min/+}$ adenomas, thereby providing potential therapeutic targets for CRC.

Material and methods

Animal experiments

$Apc^{Min/+}$ mice (strain: C57BL/6J, stock number: 002020) and *Pvillin-Cre* mice (strain: C57BL/6J, stock number: T0116) were procured from Jackson Laboratory and Model Animal Research Center (MARC), respectively. $Cul4b^{fn/fn}$ mice, previously established by our lab by flanking exons 3-5 of the *Cul4b* gene with *Loxp* sites, allowing recognition by *Cre* [20]. Subsequently, $Apc^{Min/+}$ male mice were crossbred with *Pvillin-Cre;* $Cul4b^{fn/fn}$ female mice to produce the offspring. $Apc^{Min/+}$*; Pvillin-Cre;* $Cul4b^{fn/fn}$ and $Apc^{Min/+}$*; Pvillin-Cre;* $Cul4b^{fn/Y}$ mice (referred to as $Apc^{Min/+}$*;* $Cul4b^{\Delta IEC}$) and their respective control counterparts $Apc^{Min/+}$*;* $Cul4b^{fn/fn}$ and $Apc^{Min/+}$*;* $Cul4b^{fn/Y}$ (referred to as $Apc^{Min/+}$*;* $Cul4b^{WT}$) were utilized in this study. Genomic DNA was extracted from mice tail tips using a standard proteinase K digestion method (0.1 mg/mL). Genotyping PCR was performed to determine the mouse genotype and the primers listed in Table 1. All animal experiments were conducted with approval from the Animal Care and Use Committee of the School of Basic Medical Science, Shandong University. No mice were excluded during data statistical analysis. The knockout efficiency of the included mice was confirmed through Western Blot or Immunostaining.

For tumorigenesis analysis, 4 to 5-month-old mice with matched genotypes mice were randomly chosen. The entire gastrointestinal tract was excised and divided into the colon and three segments of the small intestines: proximal, medial, and distal segments. The tissues were rinsed using cold phosphate-buffered saline (PBS) and opened longitudinally. The number and size of adenomas were determined using an OLYMPUS SZX16 microscope. Venous blood was collected into anticoagulant tubes from mice tails, and blood routine examination was conducted after a tenfold dilution with normal saline. Spleens were obtained, photographed, and weighed. For complete MDSCs, the neutralizing antibody InVivoMAb anti-mouse Ly6G/Ly6C (Gr-1) (Bio X cell, BE0075) and the control antibody InVivoMAb IgG2b (Bio X cell, BE0090) were administered intraperitoneally twice weekly at 100 μg per 20 g bodyweight in 10 to 12-week-old mice for 1 month [21,22].

Table 1
The primers for mice genotyping.

	Sequence
Cre-Forward	5′-CCCGCAGAACCTGAAGATG-3′
Cre-Reverse	5′-GACCCGGCAAAACAGGTAG-3′
Apc-1	5′-GCCATCCCTTCACGTTAG-3′
Apc-2	5′-TTCCACTTTGGCATAAGGC-3′
Apc-3	5′-TTCTGAGAAAGACAGAAGTTA-3′

Flow cytometry analysis

Adequate single cells were isolated from the spleen, peripheral blood, colon adjacent tissues, and adenoma tissues of mice. These cells were incubated with the appropriate surface antibodies: anti-CD45-PE/Cy7 (Biolegend, Cat# 103113), anti-CD3-PE/Cy7 (Biolegend, Cat# 100219), anti-CD4-FITC (Invitrogen, 11-0041-85), anti-CD8a-APC (Invitrogen, 47-0081-82), anti-CD11b-FITC (Biolegend, Cat# 101206), anti-Gr-1-PE (Biolegend, Cat# 108408), anti-CD107a-FITC (Biolegend, Cat# 121605), and anti-CD137-APC (Biolegend, Cat# 106109). For intracellular staining, cells were treated with the Fixation/Permeabilization solution (Invitrogen, 00-5223-56) overnight at 4 °C before incubating with intracellular antibodies: anti-IFNγ-PE (Biolegend, Cat# 163503). $CD4^+$ T cells were defined as $CD45^+CD4^+CD8a^-$; $CD8^+$ T cells were defined as $CD45^+CD4^-CD8a^+$; activated $CD4^+$ T cells were defined as $CD3^+CD4^+CD137^+IFN\gamma^+$; and activated $CD8^+$ T cells were defined as $CD3^+CD8a^+CD107a^+IFN\gamma^+$ [23,24]. Data acquisition was performed on an Accuri C6 Plus and analyzed using FlowJo (RRID:SCR_008520).

Chromatin Immunoprecipitation (ChIP)

ChIP was conducted using the SimpleChIP® Enzymatic Chromatin IP Kit (Cell Signaling Technology, Cat# 9003). In brief, 1×10^7 cells were cross-linked with 1.5 % formaldehyde. Subsequently, nuclei were collected, and chromatin was digested, followed by overnight incubation with 1-2 μg of the respective antibody. After mixing with magnetic beads for 2 h, the mixtures were subjected to washing steps with low and high salt buffers. Subsequently, DNA was extracted from the beads and precipitated. The enrichment of the DNA was analyzed by RT-qPCR using primers specific for the target gene promoter [25]. The antibodies used for ChIP included CUL4B (Sigma-Aldrich Cat# C9995, RRID: AB_1840781), EZH2 (Cell Signaling Technology, Cat# 5246S), H2AK119ub1 (Cell Signaling Technology, Cat# 8240S) and H3K27me3 (Cell Signaling Technology, Cat# 9733S).

Cell lines culture and viral infection

HCT116 and CT26 cell lines were procured from the cell bank of the Chinese Academy of Sciences and GeneCopoeia (Rockville, USA), respectively. HCT116 cells were cultured in McCoy's 5A medium (Sigma-Aldrich, M4892) supplemented with 20 % fetal bovine serum (AusGeneX, FBSSA500-S), penicillin (100 mg/mL, BBI, A600135) and streptomycin (100 mg/mL, BBI, A100382). CT26 cells were cultured in

Roswell Park Memorial Institute (RPMI) 1640 medium (Gibco, C11875500) supplemented with 10 % fetal bovine serum (Gibco, 10099-141C), penicillin (100 mg/mL) and streptomycin (100 mg/mL). All cell lines underwent identification and were tested using Myco-Blue Mycoplasma Detector (Vazyme, D101-02).

Cul4b knockdown (sh*Cul4b*, 5′-AATATTTCCCGGAACATTCTG-3′) and control (shNC) cells were generated by infecting cells with lentivirus. The packaging vector, including the ORF of human CUL4B was cloned into the lentiviral expression vector pLKO.1-EGFP-Puro by Dr. Yang Yang. Cells were selected using puromycin (Gibco, A1113803). For siRNA experiments, three independent siRNA sequences were tested, and the one with the highest efficiency (5′-CAGGCTCTATCGGGTATTT-3′) was employed with Lipofectamine™ 3000 (Invitrogen, L3000001) according to the manufacturer's instructions.

Adenoma organoids culture and infection

Adenoma organoids were isolated from the adenoma tissue of *Apc*$^{Min/+}$*; Cul4b*^{WT} and *Apc*$^{Min/+}$*; Cul4b*$^{\Delta IEC}$ mice. The isolation and cell dissociation of adenomas were performed as described before [26-30]. The isolation process involved dissecting adenomas from the colon, carefully cutting them, washing, and digesting them with 10 mM EDTA at 4 °C for 30 min. Subsequently, the cells were seeded in 24-well plates (Greiner bio-one, GN662102) at a density of approximately 1×10^6 cells per well. The culture medium (compositions were listed in Table 2) was refreshed every two days, and organoids were passaged at a split ratio of 1:3 every 4-7 days. For passaging, organoids were removed from Matrigel by incubating with cell recovery solution (Corning, 354253) on ice for 30 min.

The preparation of organoids and viral or plasmid infection followed established protocols[31]. Adenoma organoids were collected from Matrigel and dissociated into single cells using Trypsin-EDTA (Gibco, 25200072) for 5-15 min at 37 °C. After washing and counting, cells were resuspended in the infection mixture (lentivirus) and centrifuged in the plate at 500 × *g* for 1 h at 32 °C. Following incubation for 4-6 h at 37 °C, the cells were collected, spun down, resuspended in a mixture of Matrigel and medium, and seeded into a 24-well plate with 5×10^4 cells per well. pCMV-Tag2B Flag-CUL4B (4B-Exp, provided by Dr. Wei Jiang) and its control plasmid (Con) were transfected into Orgs^{KO} for re-expressing CUL4B, and sh*Cul4b* and control (shNC) cloned into pLKO.1-EGFP-Puro were infected with Orgs^{WT} to knockdown *Cul4b*.

Co-culture organoids with MDSCs

MDSCs were isolated from mice spleens using the Myeloid-Derived Suppressor Cell Isolation Kit (mouse, Mitenyi Biotec, 130-094-538) following the manufacturer's instructions. A single-cell suspension was obtained through digestion, resuspended in PBS buffer (0.5 % BSA, 2 mM EDTA, pH 7.2), and filtered by tissue grinding and a 30 μm filter. After cell counting, 1×10^8 cells were used per trial for subsequent processing. Following FcR blocking and anti-Ly6G-Biotin incubation, cells were treated with anti-Biotin MicroBeads. Gr-1^{high}Ly6G$^+$ cells were allowed to adsorb on an LS column (Mitenyi Biotec, 130-042-401) as the suspension passed through the MACS separator. Gr-1^{dim}Ly6G$^-$ cells were contained in the first flow-through fraction and magnetically labeled with anti-Gr-1-Biotin and Streptavidin MicroBeads. Magnetically labeled cells were immediately flushed out by firmly pushing the plunger into the column and repeating the process again. The purity of MDSCs reached 90 % using the Mitenyi Biotec 130-094-538 kit in our lab [10].

For co-culture, adenoma organoids were released from Matrigel and dissociated into single cells. After washing and counting, single cells from organoids were seeded into the lower compartment in Matrigel-pre-treated 24-well plates at a concentration of 3×10^4 cells per well. After 6 h, the obtained MDSCs were seeded on the top of the Transwell membrane (Corning, CLS3413) at a ratio of 1:1 according to the method previously described [32].

To treat with conditioned medium (CM), sterile microscope slides were pre-treated with 1 mg/mL poly-lysine at 37 °C for 2 h. MDSCs were isolated and resuspended with CM collected from the supernatant of cultured *Apc*$^{Min/+}$*; Cul4b*$^{\Delta IEC}$ and control organoids (3 days starting from 10^5 cells per well). Recombinant murine G-CSF (mG-CSF, PeproTech, 250-05, 100 ng/mL), neutralizing antibody of G-CSF (anti-G-CSF, R&D systems, MAB414, 0.5 μg/mL) and Rat IgG1 isotype control (IgG, R&D systems, MAB005, 0.5 μg/mL) were added. After incubating for 48 h, the slides were washed with PBS and fixed in ice-cold Immunol Staining Fix Solution (Beyotime, P0098) for 30 min. Following fixation, the slides were permeabilized with 0.5 % TritonX-100 in PBS, blocked for 1 h at room temperature, and incubated at 4 °C with primary antibodies overnight, followed by a secondary antibody. The primary antibodies used were anti-S100A8 and anti-S100A9, and the secondary antibody was anti-rabbit Rhodamine.

Table 2
Compositions of *Apc*$^{Min/+}$ adenoma organoids culture medium.

Component name	Concentration		Cat.
Advanced DMEM/F12		Gibco	12634010
penicillin/streptomycin	1:100	Gibco	15140122
GlutaMax	1:100	Gibco	35050-061
HEPES	1:100	Gibco	15630-080
Noggin	15 %	home-made	
N2	1x	Gibco	17502-048
B27	1x	Gibco	1704-044
N-Acetylcysteine	1.25 mM	Sigma-Aldrich	A9165
Nicotinamide	10 mM	Sigma-Aldrich	N0636
EGF	50 ng/mL	PeproTech	AF-100-15
Y-27632	10 μM	SELLECK	S6390
A83-01	500 nM	Tocris	2939
SB202190	3 μM	Sigma-Aldrich	S7067
Gastrin	10 nM	Tocris	3006
Primocin	1x	Invitrogen	ant-pm-1

Database analysis

The Spearman correlation analyses were conducted using TIMER2.0 (http://timer.comp-genomics.org) to assess the correlation between *CUL4B* and *CSF3* in colorectal adenocarcinoma (COAD), lung adenocarcinoma (LUAD) and prostate adenocarcinoma (PRAD) based on The Cancer Genome Atlas (TCGA) data. To further explore the enrichment of genes associated with MDSCs in GDS2947, enrichment analyses were carried out using Bioinformatics (http://www.bioinformatics.com.cn), and the Spearman correlation analyses between *CUL4B* and *CD84* using TIMER2.0.

Statistical analysis

The experimental procedures were conducted with biological or independent replicates, and statistical analyses were carried out using GraphPad Prism. The genotype information was not disclosed during the analysis. Data significance was determined using unpaired *t*-tests and ANOVA analysis. Bar graphs were used to represent mean ± SEM. *p*-values were denoted as follows: *<0.05, **<0.01, ***<0.001, ****<0.0001, and "ns" indicated not significant.

Other methods and materials were provided in supporting information Supplementary Doc.

Results

Deletion of Cul4b in the gut epithelium promotes Apc$^{Min/+}$ *adenoma formation*

CUL4B has recently emerged as a novel regulator influencing gut self-renewal and intestinal stem cells (ISCs) [33]. In an effort to

elucidate the precise role of CUL4B in the early stages of CRC carcinogenesis, we leveraged the tumor-prone genetic background of the $Apc^{Min/+}$ model to examine how CUL4B impacts $Apc^{Min/+}$ adenoma formation. By crossing $Apc^{Min/+}$ mice with our previously established *Pvillin-Cre; Cul4b*$^{fn/fn}$ mice [20], we generated offspring with ($Apc^{Min/+}$; *Cul4b*$^{\Delta IEC}$) or without ($Apc^{Min/+}$; *Cul4b*^{WT}) *Cul4b* deletion in gut epithelium (Fig. S1A). As anticipated, a substantial loss of CUL4B, but not its homologue CUL4A, was verified through immunofluorescent staining and immunoblotting in $Apc^{Min/+}$; *Cul4b*$^{\Delta IEC}$ mice (Fig. 1A-B, Fig. S1B-S1C). The immunoblot detection of residual CUL4B expression in the knockout tissue was attributed to its presence in non-epithelial cells.

Upon spontaneous loss of the second *Apc* allele, the adenomatous polyposis mutation resulted in aberrant activation of Wnt signaling, leading to the induction of adenoma formation. $Apc^{Min/+}$; *Cul4b*$^{\Delta IEC}$ mice exhibited an accelerated progression in adenoma formation, evidenced by an increased number of adenomas (with size above 2 mm) in both the colon and intestinal segments (Fig. 1C-D, Fig. S1D-S1G). Correspondingly, $Apc^{Min/+}$; *Cul4b*$^{\Delta IEC}$ mice displayed severe splenomegaly and anemia due to heightened tumorigenicity (Fig. 1E-F). Although there was an accelerated propensity for death, no significant difference was observed in the survival rate of *Cul4b*-knockout mice (Fig. 1G). The impact of CUL4B loss on adenoma genesis observed in $Apc^{Min/+}$ mice was consistent across genders (Fig. 1H). These findings suggest that CUL4B deficiency promotes both the initiation and progression of adenomas in the context of $Apc^{Min/+}$.

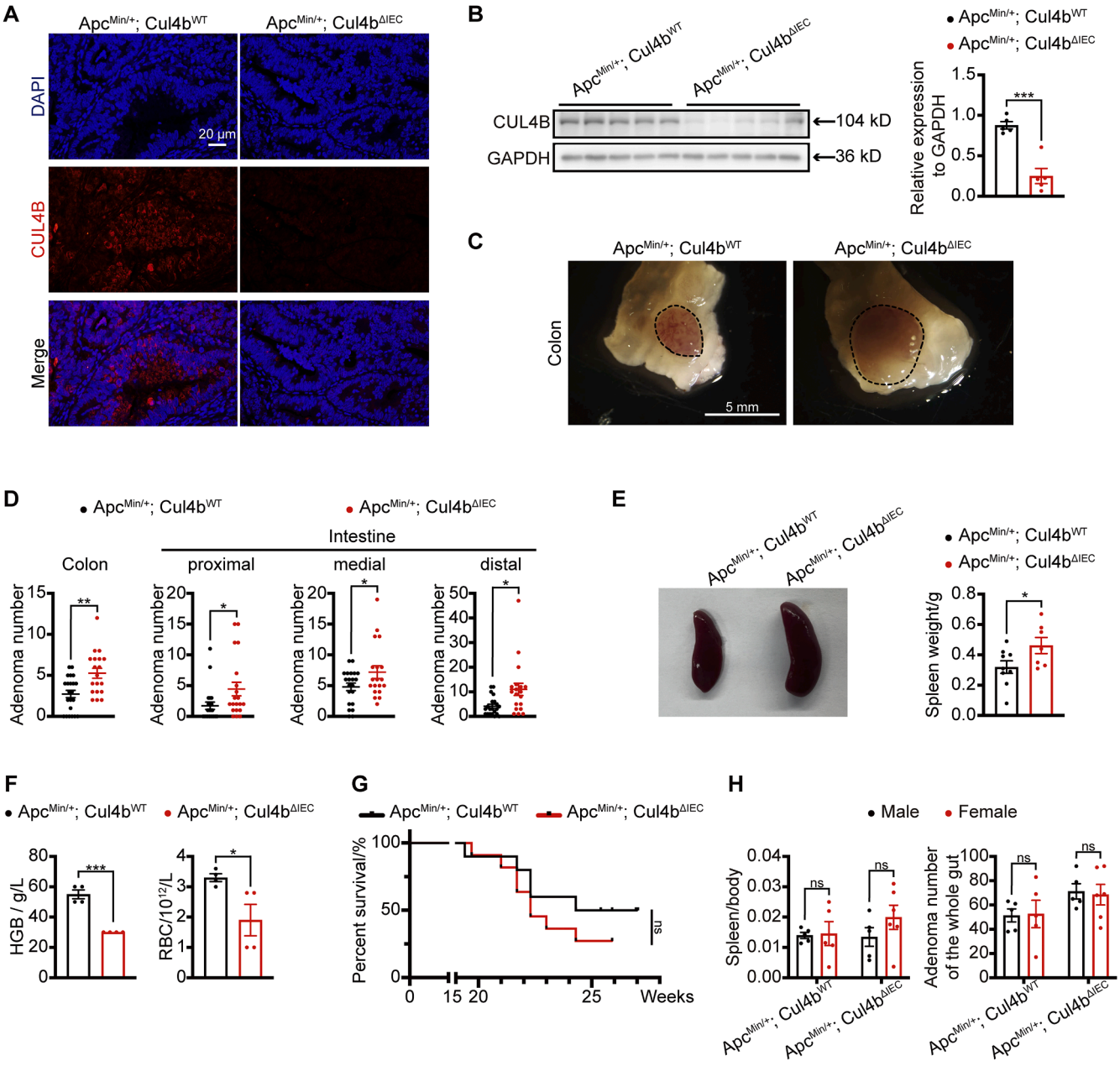

Fig. 1. Loss of CUL4B in gut epithelium encourages $Apc^{Min/+}$ adenoma formation. (A) Representative images of immunostaining of CUL4B in adenoma tissues (3 vs. 3). Red indicates CUL4B; Blue indicates DAPI. (B) Western Blot analysis of CUL4B for characterization of the knockout efficiency. (C) Representative images of adenoma tissue (9 vs. 9). Dotted lines indicate adenomas. (D) Total number of adenomas with size > 2 mm in proximal, medial, and distal segments of the intestine and colon (21 vs. 19). All mice were 5 months old. (E) Representative images and statistical assessment of spleen weight (9 vs. 7). (F) Examination of peripheral blood (4 vs. 4). HGB: hemoglobin; RBC: red blood cells. (G) Kaplan-Meier survival examination (10 vs. 11). (H) Spleen weight and count of adenomas across the whole gut were examined in grouped male and female $Apc^{Min/+}$; *Cul4b*$^{\Delta IEC}$ and $Apc^{Min/+}$; *Cul4b*^{WT} mice (5 vs. 5).

Inhibition of CUL4B enhances $Apc^{Min/+}$ adenoma growth through tumor microenvironment

The frequent occurrence of loss of heterozygosity (LOH) at *APC* genetic loci during the pre-tumor stage is well-documented [34,35]. To delve into the root cause of adenoma development following *Cul4b* deletion, we initially conducted PCR and DNA sequencing to examine whether LOH was altered in adenomas from $Apc^{Min/+}$; $Cul4b^{\Delta IEC}$ and control mice using mismatched primers. The *Apc* allele was deleted in all randomly selected adenomas from both groups (Fig. S2), indicating that CUL4B deficiency did not impact LOH. Further investigations involved the generation of *in vitro* epithelial organoids derived from $Apc^{Min/+}$; $Cul4b^{\Delta IEC}$ and control adenomas [28–30]. As illustrated in Fig. 2A and B, CUL4B expression was virtually undetectable in $Apc^{Min/+}$; $Cul4b^{\Delta IEC}$ organoids. However, contrary to the *in vivo* phenotype, *Cul4b*-deficient adenomas unexpectedly formed much smaller organoids with a lower formation frequency (Fig. 2C-D). These findings suggest that the lack of TME *in vitro* is likely responsible for the diminished epithelial organoids observed with CUL4B ablation.

Subsequently, we conducted RNA sequencing (RNA-seq) to obtain transcriptional profiles of paired adenomas and adjacent tissues with or without *Cul4b* deletion. At Stages I (90 days, initiation), II (120 days), and III (150 days), 1049, 882, and 360 differentially expressed genes (DEGs, fold change > 2, $p < 0.05$) were identified in adenomas, respectively. Meanwhile, 2251, 761, and 312 DEGs were found in adjacent tissues at different stages (Fig. 2E). Given that CUL4B ablation predominantly led to DEGs in the early phase of $Apc^{Min/+}$ adenoma initiation, we performed gene ontology (GO) analysis of DEGs in adjacent tissue at Stage I. Multiple immune-related annotations were enriched in $Apc^{Min/+}$; $Cul4b^{\Delta IEC}$ tissues, including negative regulation of the immune system process and positive regulation of cytokine secretion (Fig. 2F), suggesting alterations in the tumor-associated immune microenvironment following *Cul4b* deletion.

Loss of CUL4B encourages the recruitment of MDSCs in the tumor microenvironment

Subsequently, we employed flow cytometry and immunostaining to dissect the specific cell populations affected in the immune microenvironment due to *Cul4b* knockout. Adenomas with diameters exceeding 2 mm were chosen for analysis to mitigate the impact of tumor size on the recruitment of tumor-infiltrating cells. Positive staining of CD45, representing nearly all immunological and hematological cells, exhibited comparable levels between the two groups (Fig. S3A). However, $CD11b^{+}Gr\text{-}1^{+}$ MDSCs, as opposed to other infiltrating immune cell populations, were significantly enriched in both $Apc^{Min/+}$; $Cul4b^{\Delta IEC}$ adenomas and adjacent tissue (Fig. 3A-B, Fig. S3B-S3C). No notable differences were observed in the analysis of immune cell populations from peripheral blood or spleen (Fig. S3D-S3I). To further corroborate the findings, CD84, a recently identified specific surface marker defining MDSCs, and S100A8 and S100A9, two proteins correlated with MDSCs, were also elevated in $Apc^{Min/+}$; $Cul4b^{\Delta IEC}$ adenomas (Fig. 3C-F).

Given the association of increased MDSCs with T cell repression [36–40], we further assessed tumor-activated T cells and observed a slight decrease in tumor-infiltrating cytotoxic $CD8^{+}$ T cells (Fig. 3G, Fig. S3J). Upregulation of PD-1/PD-L1 expression within $Apc^{Min/+}$; $Cul4b^{\Delta IEC}$ adenomas was also confirmed (Fig. 3H). In aggregate, the loss of CUL4B was found to promote the accumulation of MDSCs, creating a microenvironment conducive to adenoma development. To validate this, we employed an anti-mouse Ly6G/Ly6C (Gr-1) neutralizing antibody through intraperitoneal injection. The functionality of the neutralizing antibody was verified without altering CUL4B expression (Fig. 3I-J). It was demonstrated that the blockade of Ly6G/Ly6C (Gr-1) reduced adenoma growth and S100A8 expression in *Cul4b* deletion mice (Fig. 3K-L). These findings suggest that neutralizing the function of MDSCs rescued the tumor-prone microenvironment, leading to decreased adenoma formation.

CUL4B-deficient adenomas enhance migration and activity of MDSCs

To further verify the impact of CUL4B on MDSCs recruitment, we collected supernatant from a comparable number of cultured adenoma organoids with or without *Cul4b* deletion as conditioned medium (CM^{WT} or CM^{KO}). Subsequently, we examined the migration behavior of wild-type MDSCs treated with either CM^{KO} or CM^{WT} using Transwell migration assays. As illustrated in Fig. 4A-D, an increase in migrated MDSCs and elevated expression of S100A8/9, as well as *Nos2, Arg1* and *Csf3r* were observed after CM^{KO} treatment, suggesting that CUL4B-deleted cells enhance MDSCs migration through soluble factors.

To ascertain whether the deficiency of MDSCs in organoids explains the reverse effect of CUL4B deficiency *in vitro* and *in vivo*, we replenished isolated MDSCs into organoids. A co-culture system was established by growing wild-type or *Cul4b*-deficient organoids on coated Matrigel with wild-type MDSCs on the upper Transwell (illustrated in Fig. 4E). After 96 h of co-culture, the reduced colony number of *Cul4b*-deficient adenoma organoids was significantly rescued (Fig. 4F-G). Additionally, the decreased expression of tumor cell-secreted MDSCs-inducing factors (*Il6* and *Cox2*) [41–44] was also markedly rescued after co-culture (Fig. 4H). These findings suggest the potential instructive effect of $Apc^{Min/+}$; $Cul4b^{\Delta IEC}$ adenoma cells on MDSCs.

Deletion of CUL4B epigenetically upregulates Csf3 expression

To identify tumor-cell secreted factors responsible for recruiting MDSCs, such as G-CSF, GM-CSF, interleukins and chemokines [45], we performed RT-qPCR to screen the expression of reported chemokines in *Cul4b* knockout and control adenomas. We observed that *Csf3*, a gene encoding G-CSF, was increased in *Cul4b*-deficient adenomas (Fig. S4A). Elevated G-CSF was confirmed at the mRNA level in organoids (Fig. 5A) and at the secreted protein level in the supernatant by ELISA tests (Fig. 5B). Knockdown of *CUL4B* in human HCT116 and murine CT26 cancer cell lines also led to an increase in G-CSF (Fig. S4B-S4C). To further strengthen these observations, rescue experiment was performed and found that re-introduction of CUL4B into $Orgs^{KO}$ and knockdown *Cul4b* in $Orgs^{WT}$ reversed the expression of G-CSF, thereby inverting the migration and activation of MDSCs with the predictable expression changes of S100A8/A9 (Fig. 5C-G).

To confirm whether *Cul4b* knockout organoids affected MDSCs through G-CSF, we added recombinant G-CSF into CM^{WT} and neutralizing antibody of G-CSF into CM^{KO} predictably emphasized the mediated role of G-CSF owing to the remarkable reversal of activation markers of MDSCs (Fig. 5H-I, Fig. S4D). Furthermore, we interfered with *Csf3* using siRNA transfection (Fig. S4E-S4G). Treatment with conditioned medium obtained from organoids after *Csf3* knockdown reduced the increased migration capacity and the activated expression of S100A8/9 in MDSCs (Fig. 5J-L). Meanwhile, the knockdown of *Csf3* in *Cul4b*-deficient organoids led to increased colony number after co-cultured with MDSCs, with no significant change in size (Fig. 5M, Fig. S4H).

Mechanistically, we next examined whether CUL4B bound to the promoter of the *Csf3* gene by quantitative ChIP assay using a series of primers. A binding peak was found at -1561 bp to -1338 bp upstream of the transcription start site (TSS) of the *Csf3* promoter (Fig. 6A, Fig. S5A). Given that CRL4B has been reported to coordinate with the polycomb repressive complex 2 (PRC2), we further detected the changes in histone modification and found that deletion of *Cul4b* resulted in a marked decrease in EZH2 and consequently decreased H3K27me3 and H2AK119ub1 at the binding peak (Fig. 6B, Fig. S5B). Furthermore, treatment with the EZH2 inhibitor Dznep upregulated the expression of G-CSF (Fig. 6C-D), providing evidence that CUL4B coordinates with the PRC2 to repress the transcription of the *Csf3* gene. In conclusion, the deletion of CUL4B increased MDSCs accumulation through transcriptionally derepressing *Csf3* expression.

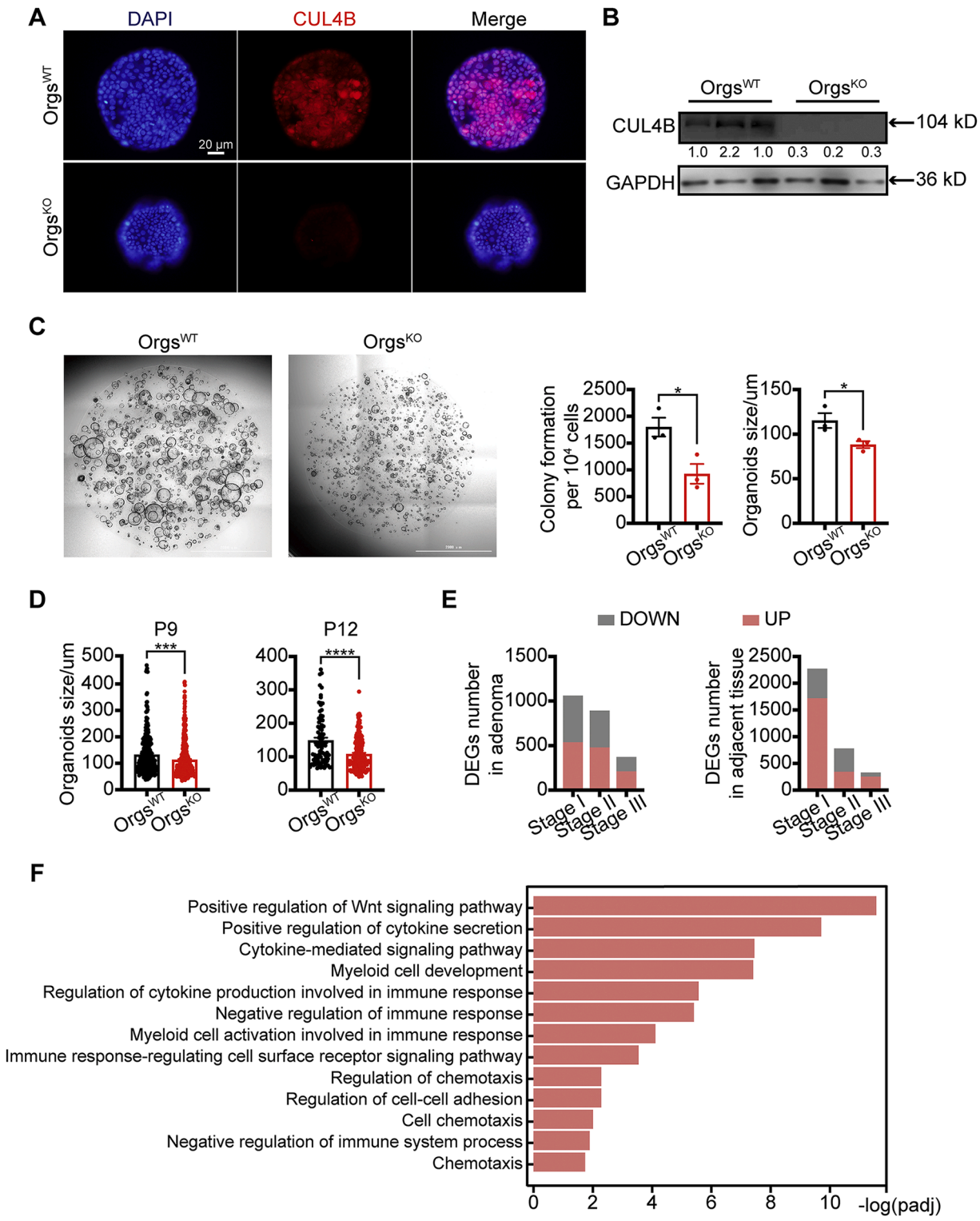

Fig. 2. Repressing CUL4B exacerbates *Apc*$^{Min/+}$ adenoma growth through the tumor microenvironment. (A) Representative images of immunostaining of CUL4B in organoids (Orgs) (3 vs. 3). Red indicates CUL4B; Blue indicates DAPI. (B) Western Blot assessment for characterization of the knockout efficiency of CUL4B in Orgs. (C) Representative bright field images and statistical analysis of Orgs formation as well as the size of Orgs. (D) Size of Orgs^{WT} and Orgs^{KO} at passages 9 and 12 compared using a single cell assay. Three independent experiments were conducted in triplicate. (E) Statistical analysis of the number of DEGs in an adenoma and adjacent tissue from Stage I, Stage II, and Stage III mice. (F) GO analysis of DEGs characterized via RNA-seq from *Apc*$^{Min/+}$; *Cul4b*$^{\Delta IEC}$ and *Apc*$^{Min/+}$; *Cul4b*^{WT} mice at Stage I.

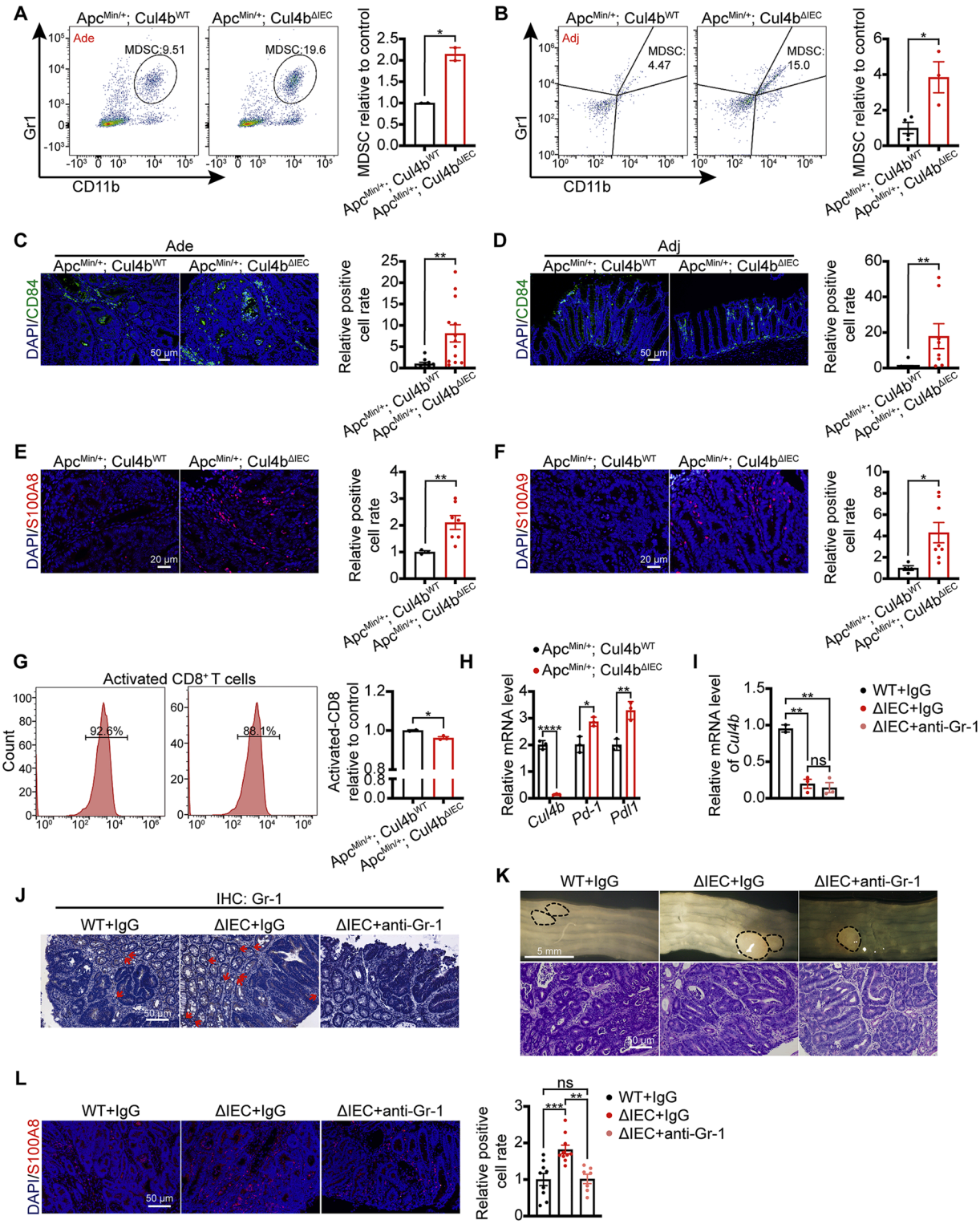

Fig. 3. The loss of CUL4B recruits increases MDSCs to promote the progression of adenoma. (A-B) Flow cytometry examination of $CD11b^{+}Gr\text{-}1^{+}$ MDSCs in adenomas (A, Ade) as well as adjacent normal tissues (B, Adj). (C-D) Representative images and statistical analyses of immunostaining of MDSCs marker CD84 in Ade (C) and Adj (D). Green indicates CD84; Blue indicates DAPI. (E-F) Representative images and statistical analyses of immunostaining of S100A8 (E) and S100A9 (F) in adenoma. Red indicates S100A8/S100A9; Blue indicates DAPI. (G) Flow cytometry assessment of activated $CD8^{+}$ T cells within adenoma. (H) The *Pd-1* and *Pdl1* mRNA levels in adenoma. (I) The knockout efficiency of *Cul4b* in mice after administration of a neutralizing antibody (anti-Gr-1). (J) Representative images of immunostaining of Ly6G/Ly6C (Gr-1) aiming to detect the blocking efficiency. Red arrows denote positive staining. (K) Representative images of the adenomas and H&E staining of adenoma. Dotted lines denote adenomas in the colon. (L) Representative images and statistical analyses of immunostaining of S100A8 of adenoma. Red indicates S100A8; Blue indicates DAPI.

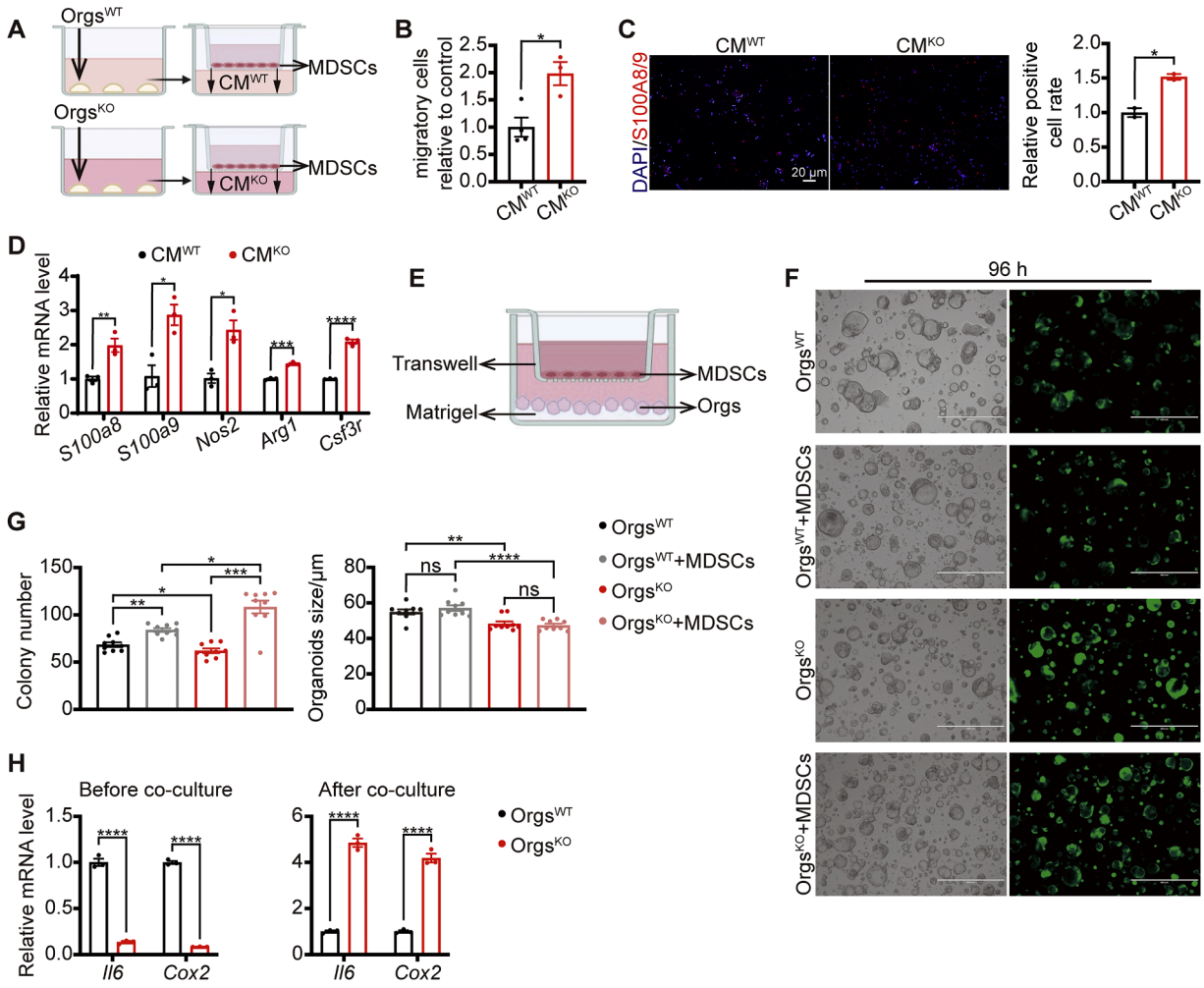

Fig. 4. *In vitro* co-culture of CUL4B-deficient adenoma organoids improves the migration and activity of MDSCs. (A) Illustration of MDSCs migration assay when treated with CM. (B) Calculation of MDSCs undergoing migration in the migration assay treated with CM^{WT} and CM^{KO} for 3 h. Four independent experiments were performed. (C) Representative images and statistical analyses of immunostaining of S100A8/9 of MDSCs administered CM^{WT} and CM^{KO} for 48 h. Red indicates S100A8/9; Blue indicates DAPI. (D) The mRNA levels of *S100a8, S100a9, Nos2, Arg1* and *Csf3r* from MDSCs treated with CM^{WT} (n=3) and CM^{KO} (n=3) for 48 h. (E) Illustration of co-culture of wild-type MDSCs and GFP-labeled $Orgs^{WT}$ and $Orgs^{KO}$. (F) Representative bright field and fluorescent images of co-cultured Orgs after co-culturing for 96 h. Scale bar: 400 μm. (G) Colony formation number and size of $Orgs^{WT}$ and $Orgs^{KO}$ following co-culture. Three independent experiments were conducted. (H) The mRNA expression of *Il6* and *Cox2* across the Orgs before and after co-culturing.

The negative correlation between CUL4B and CSF3 expression in CRC patients

We conducted a comprehensive analysis of adenoma clinical databases from the Cancer Genome Atlas (TCGA) to explore the association between CUL4B and *CSF3* expression in CRC patients and other adenocarcinomas. *CUL4B* exhibited a negative correlation with *CSF3* in colorectal adenocarcinoma (COAD) (Fig. 7A), as well as in lung adenocarcinoma (LUAD) and prostate adenocarcinoma (PRAD) (Fig. 7B-C). Cumulative survival analysis revealed that high *CSF3* expression was associated with a propensity for poor survival (Fig. 7D). Additionally, we examined GDS2947, a database focused on colorectal adenoma and normal mucosa from 32 patients. The heatmap showed the expressional profiles of main chemokines associated with MDSCs, defined marker of MDSCs and CUL4B in a clinical data of normal mucosa and adenomas (Fig. 7E). A significant negative was found between the expression of *CUL4B* and *CD84*, a defined marker of MDSCs (Fig. 7F). These data further suggest the association of CUL4B with MDSCs in patients.

Conclusions

In summary, our investigation demonstrates that the deletion of CUL4B in gut epithelium upregulates G-CSF expression, thereby increasing MDSCs recruitment and fostering a tumor-prone environment, ultimately promoting $Apc^{Min/+}$ adenoma formation (Fig. 7G).

Discussion

Tumor initiation, particularly in CRC, involves a complex interplay of genetic and epigenetic alterations that drive uncontrolled tumor cell proliferation while evading immune surveillance, allowing the evasion of antitumor responses [46]. CUL4B is known for promoting tumor cell proliferation, migration, invasion, and tumorigenesis, has garnered attention due to emerging evidence suggesting a contrasting role in inhibiting tumors, particularly in hematopoietic cells [9,10]. Our study adds a significant layer to this understanding by revealing that the deletion of CUL4B in gut epithelium expedites $Apc^{Min/+}$ adenoma formation through the recruitment of MDSCs. Intriguingly, our recent work also underscores a similar function of CUL4B in lung epithelial cells, where its deficiency promotes the development of KRAS-mutated lung

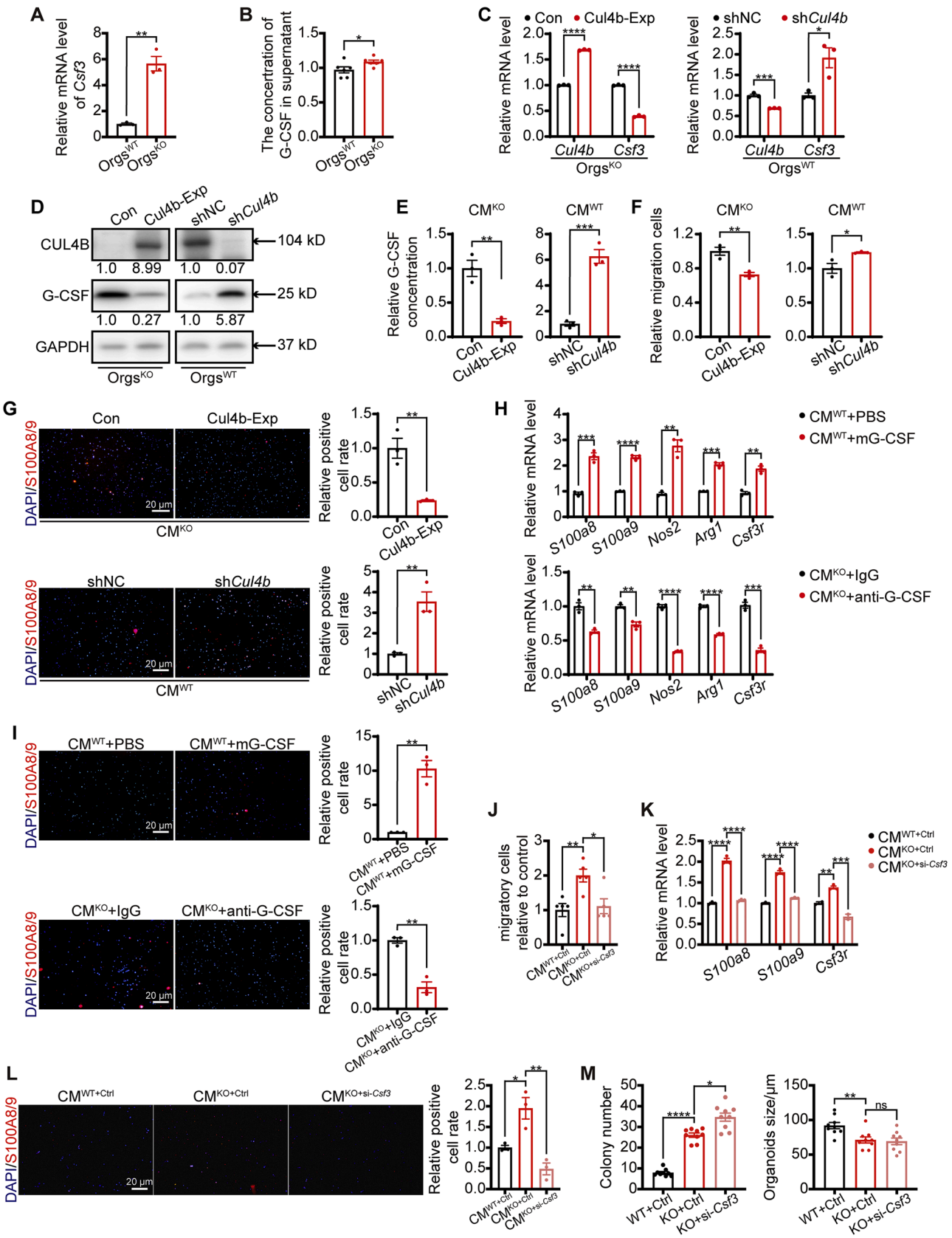

(caption on next page)

Fig. 5. CUL4B functions on MDSCs through inhibiting G-CSF . (A) The mRNA level of *Csf3* across the Orgs. (B) ELISA of secreted G-CSF in the sampled cell supernatant using a consistent number of cells from Orgs. Three independent experiments were carried out in triplicate wells. (C-D) The overexpression efficiency of G-CSF in $Orgs^{KO}$ and knockdown efficiency of G-CSF in $Orgs^{WT}$ tested using RT-qPCR (C) and Western Blot (D). (E) ELISA of secreted G-CSF after re-introduction CUL4B into $Orgs^{KO}$ and knockdown *Cul4b* in $Orgs^{WT}$. (F) Determination of migrated MDSCs treated with CM^{KO} after re-introduction CUL4B and CM^{WT} after knockdown *Cul4b*. (G) Representative images and statistical analyses of immunostaining of S100A8/9 of MDSCs treated with CM^{KO} after re-introduction CUL4B and CM^{WT} after knockdown *Cul4b*. (H) The mRNA level of *S100a8, S100a9, Nos2, Arg1* and *Csf3r* of MDSCs treated with CM^{WT} added murine G-CSF (CM^{WT}+mG-CSF) and CM^{KO} added neutralizing antibody of G-CSF (CM^{KO}+anti-G-CSF). (I) Representative images and statistical analyses of immunostaining of S100A8/9 of MDSCs treated with CM^{WT}+mG-CSF and CM^{KO}+anti-G-CSF. (J) Determination of migrated MDSCs using the migration assay after treatment with $CM^{WT+Ctrl}$, $CM^{KO+Ctrl}$, and $CM^{KO+si\text{-}Csf3}$ via counting. Three independent experiments were conducted. (K) Identification of the mRNA level of *S100a8, S100a9*, and *Csf3r* of MDSCs administered $CM^{WT+Ctrl}$ (n=3), $CM^{KO+Ctrl}$ (n=3), and $CM^{KO+si\text{-}Csf3}$ (n=3) for 48 h. (L) Representative images and statistical analyses of immunostaining of S100A8/9 of MDSCs treated with $CM^{WT+Ctrl}$, $CM^{KO+Ctrl}$, and $CM^{KO+si\text{-}Csf3}$. Three independent experiments were conducted. (M) Colony formation number and size of organoids in pre-knockdown *Csf3* organoids following 96 h of co-culture. Three independent experiments were conducted.

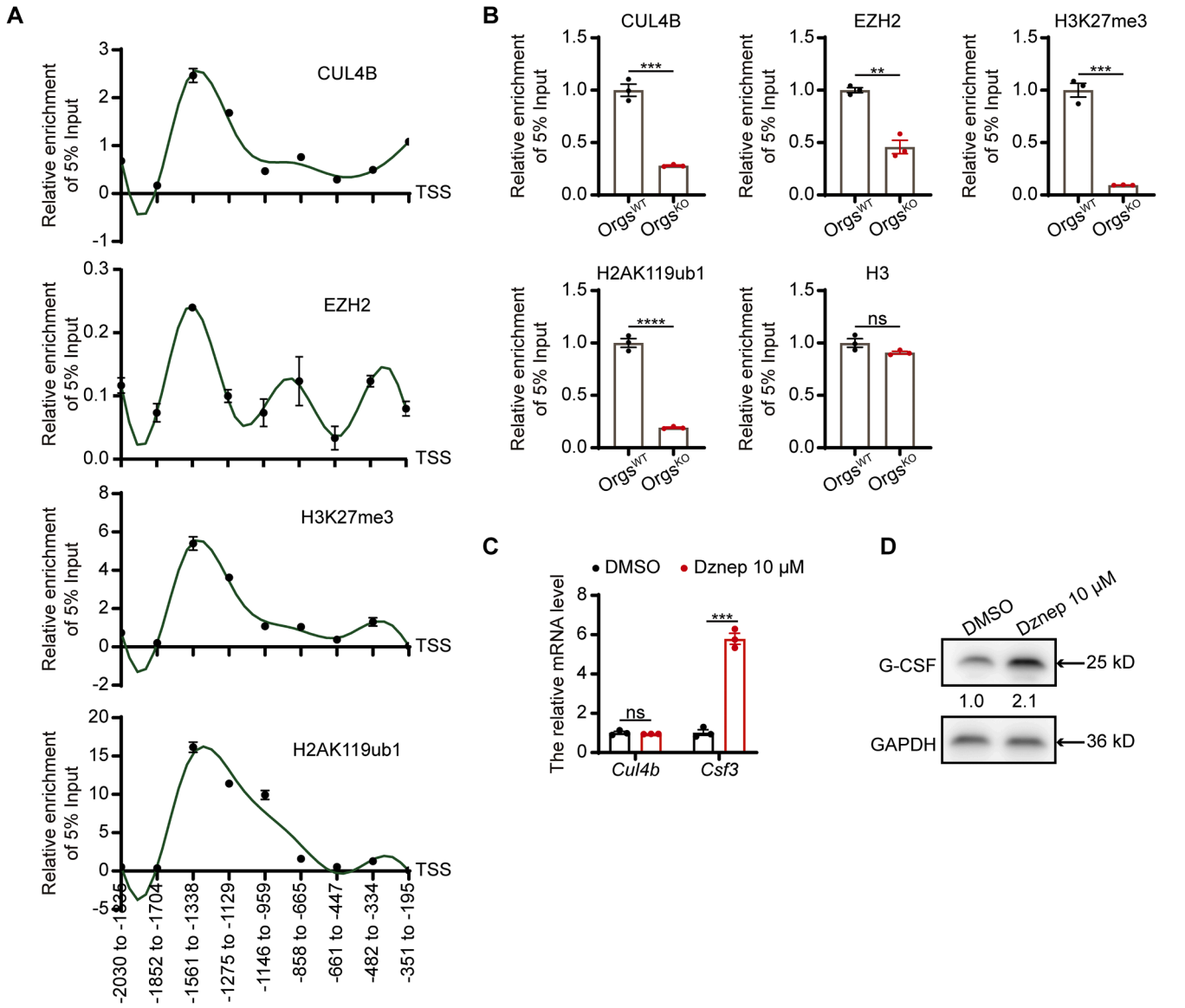

Fig. 6. CUL4B binds to the promotor of *Csf3* gene and transcriptionally represses its expression. (A) qPCR following ChIP to investigate the binding of CUL4B, EZH2, H3K27me3 and H2AK119ub1 to the *Csf3* promoter in organoids using a collection of primers. (B) qPCR following ChIP to examine alterations in CUL4B, EZH2, H3K27me3 and H2AK119ub1, and associated with the *Csf3* promoter (-1561 bp to -1338 bp) using Histone 3 as a control. (C-D) The mRNA (C) and protein level (D) of G-CSF after treating with Dznep (EZH2 inhibitor, 10 μM, 48 h).

adenocarcinoma by enhancing MDSCs accumulation [47].

CRC stands out as a leading cause of global cancer-related mortality, primarily initiated by the permanent activation of the Wnt pathway and involving intricate interactions with immune cells. To identify potential novel therapeutic targets for CRC, it is crucial to delve into the regulatory roles of genes, especially in the context of *Apc* mutation. Our study provides a multifaceted exploration of the impact of CUL4B deletion in gut epithelium on $Apc^{Min/+}$ adenoma formation.

Firstly, the loss of CUL4B in gut epithelium emerges as a promoter of adenoma formation within the genetic background of Wnt-disturbed *Apc*

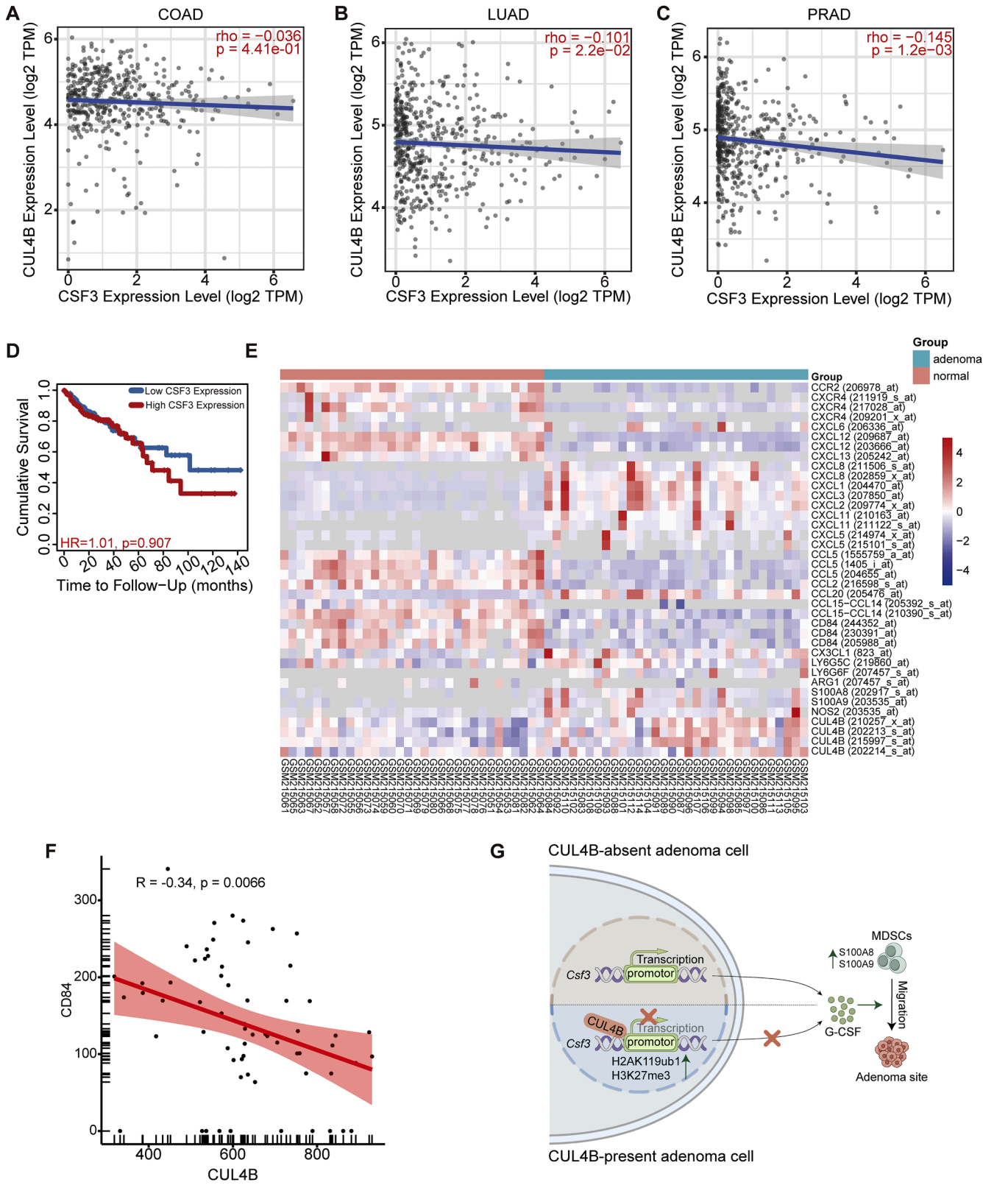

Fig. 7. Negative relationship between *CUL4B* and *CSF3* expression in diverse adenoma types. (A-C) The Spearman correlation analysis of the expression of *CUL4B* and *CSF3* in COAD (A), LUAD (B) and PRAD (C) from TCGA. (D) The cumulative survival analysis associated with the expression of *CSF3* in COAD. (E) The heatmap of genes associated with MDSCs in GDS2947 determined through bioinformatic analysis. (F) The Spearman correlation analysis of the expression of *CUL4B* and *CD84* in GDS2947. (G) Deletion of gut epithelial CUL4B promotes to recruit MDSCs by regulating G-CSF transcriptionally.

mutants, predominantly through the recruitment of tumor-infiltrating MDSCs. The rescue of adenoma growth through intraperitoneal injection of Ly6G/Ly6C (Gr-1) neutralizing antibody strongly suggests that the effects of CUL4B deletion on $Apc^{Min/+}$ tumorigenesis are intricately linked to the accumulation of MDSCs.

Secondly, our investigation unveils a novel mechanism wherein CUL4B binds to the promoter of *Csf3*, actively suppressing the transcription of G-CSF, a key recruiter of MDSCs, by modulating histone modifications, specifically H3K27 trimethylation and H2AK119 monoubiquitylation. This regulatory role of CUL4B adds a layer of complexity to its functions in the context of CRC progression.

Thirdly, our *in vitro* organoid culture model provides additional support, demonstrating that CUL4B-deleted cells secrete elevated levels of G-CSF. Interfering with *Csf3* reverses the phenotypes observed in CUL4B knockout organoids co-cultured with MDSCs, underscoring the critical role of the microenvironmental cellular context.

Moreover, the analysis of CUL4B and MDSCs' relative markers in the COAD database from TCGA and GDS2947 consistently supports our findings, affirming that *CUL4B* acts as a tumor-suppressor gene during CRC progression.

MDSCs, characterized by the surface expression of CD11b and Gr-1, constitute a diverse population of immature monocytes and granulocytes that have been observed to accumulate both in primary tumor sites and metastatic locations [48]. The recruitment of myeloid precursors, a pivotal event in MDSCs accumulation, is influenced by tumor-derived suppressor factors (TDSFs), including G-CSF [49], GM-CSF [50], IL-6 [42], and COX2 [51]. In our investigation, we observed a significant upregulation of *Csf3* at the mRNA level in CUL4B deletion mice, among several reported MDSCs chemokines. MDSCs play a crucial role in the immunosuppressive milieu of CRC, and their migration to CRC foci or liver tissue is facilitated by signaling axes such as KRAS-IRF2-CXCL3 and VEGF-CXCL1 [52,53]. Additionally, the PGE2-EP4 signaling axis promotes MDSCs differentiation [54]. Our findings support a novel mechanism wherein the deficiency of CUL4B in epithelial cells robustly recruits MDSCs through G-CSF in CRC, shedding light on an unexplored facet of CRC pathogenesis.

Notably, organoids derived from adenomas displayed a marked reduction in organoid formation ability and size upon *Cul4b* knockout, presenting a contrast to the *in vivo* effects of *Cul4b* knockout. This disparity may be attributed to the absence of a microenvironmental matrix in organoid culture systems. The inconsistent phenotypes were rescued by the introduction of MDSCs, leading to the reversal of *Il6/Cox2* expression in organoids following co-culture. Exosomal S100A9 transfer from MDSCs has been reported to enhance the expression of stemness markers and promote sphere formation in CRC cells [55], hinting at the existence of critical secreted factors between MDSCs and CRC cells. This aspect warrants further exploration in our future research.

In conclusion, our study unveils a novel role of gut epithelial CUL4B in a mouse model of *Apc*-induced tumor initiation and progression. Mechanistically, we demonstrate that the deletion of CUL4B transcriptionally upregulates G-CSF expression (Fig. 7G). Our results highlight the hitherto undiscovered function of CUL4B in suppressing colon adenoma formation to create a tumor-permissive microenvironment, offering a potential therapeutic strategy for treating CRC.

Data availability statement

The genomic data (RNA-seq) has been deposited into the Gene Expression Omnibus (GEO) database: GSE189382. All the other datasets and code are available upon request from huhuili@sdu.edu.cn.

Funding

This work was supported by the grants from: the National Key R&D Program of China 2019YFA0111400, 2018YFA0507900, the National Natural Science Foundation of China 32122031, 92068121, 31970779, and 31970559, the Funds for Taishan Youth Expert of Shandong Province, Shandong Province National Outstanding Young Scholars Foundation ZR2021JQ11, Youth Interdisciplinary Innovation Research Group of Shandong University 2020QNQT003 and Key Research and Development Program of Shandong Province 2022CXGC020501.

Ethics approval and consent to participate

All animal experiments were performed in compliance with associated guidelines and have been approved by the Animal Care and Use Committee of the School of Basic Medical Science, Shandong University (approval number: KYLL-2017(KS)-363).

CRediT authorship contribution statement

Beibei Guo: Data curation, Formal analysis, Investigation, Methodology, Validation, Visualization, Writing – original draft. **Yawen Zheng:** Data curation, Formal analysis. **Yujia Fan:** Methodology. **Yang Yang:** Formal analysis, Methodology. **Yuxing Wang:** Methodology. **Liping Qin:** Methodology. **Yachun An:** Methodology. **Xiaoran Xu:** Methodology. **Xiyu Zhang:** Methodology, Project administration, Resources, Supervision. **Gongping Sun:** Methodology, Project administration, Resources, Supervision. **Hao Dou:** Methodology, Project administration, Resources, Supervision. **Changshun Shao:** Methodology, Project administration, Resources, Supervision. **Yaoqin Gong:** Conceptualization, Funding acquisition, Methodology, Project administration, Resources, Supervision. **Baichun Jiang:** Conceptualization, Methodology, Project administration, Resources, Supervision. **Huili Hu:** Conceptualization, Funding acquisition, Methodology, Project administration, Resources, Supervision, Writing – original draft, Writing – review & editing.

Declaration of competing interest

The authors declare that they have no known competing financial interests or personal relationships that could have appeared to influence the work reported in this paper.

Acknowledgments

We sincerely thank Professor Hans Clevers for kindly providing the cell lines to produce recombinant Noggin. We thank Professor Bo Han for clinical support. We thank Translational Medicine Core Facility of Shandong University for consultation and instrument availability that supported this work.

Supplementary materials

Supplementary material associated with this article can be found, in the online version, at doi:10.1016/j.neo.2024.101005.

References

[1] J. Hannah, P. Zhou, Distinct and overlapping functions of the cullin E3 ligase scaffolding proteins CUL4A and CUL4B, Gene 573 (1) (2015) 33–45, https://doi.org/10.1016/j.gene.2015.08.064.
[2] C. Kerzendorfer, L. Hart, R. Colnaghi, G. Carpenter, D. Alcantara, E. Outwin, et al., CUL4B-deficiency in humans: understanding the clinical consequences of impaired Cullin 4-RING E3 ubiquitin ligase function, Mech. Ageing Dev. 132 (8-9) (2011) 366–373, https://doi.org/10.1016/j.mad.2011.02.003.
[3] Y. Li, H. Hu, Y. Wang, Y. Fan, Y. Yang, B. Guo, et al., CUL4B contributes to cancer stemness by repressing tumor suppressor miR34a in colorectal cancer, Oncogenesis. 9 (2) (2020) 20, https://doi.org/10.1038/s41389-020-0206-3.
[4] X. Liu, J. Cui, L. Gong, F. Tian, Y. Shen, L. Chen, et al., The CUL4B-miR-372/373-PIK3CA-AKT axis regulates metastasis in bladder cancer, Oncogene 39 (17) (2020) 3588–3603, https://doi.org/10.1038/s41388-020-1236-1.

[5] M. Zhao, M. Qi, X. Li, J. Hu, J. Zhang, M. Jiao, et al., CUL4B/miR-33b/C-MYC axis promotes prostate cancer progression, Prostate 79 (5) (2019) 480–488, https://doi.org/10.1002/pros.23754.

[6] H. Hu, Y. Yang, Q. Ji, W. Zhao, B. Jiang, R. Liu, et al., CRL4B catalyzes H2AK119 monoubiquitination and coordinates with PRC2 to promote tumorigenesis, Cancer Cell 22 (6) (2012) 781–795, https://doi.org/10.1016/j.ccr.2012.10.024.

[7] Y. Yang, R. Liu, R. Qiu, Y. Zheng, W. Huang, H. Hu, et al., CRL4B promotes tumorigenesis by coordinating with SUV39H1/HP1/DNMT3A in DNA methylation-based epigenetic silencing, Oncogene 34 (1) (2015) 104–118, https://doi.org/10.1038/onc.2013.522.

[8] P.J. Duan, J.H. Zhao, L.L. Xie, Cul4B promotes the progression of ovarian cancer by upregulating the expression of CDK2 and CyclinD1, J. Ovarian. Res. 13 (1) (2020) 76, https://doi.org/10.1186/s13048-020-00677-w.

[9] Y. Qian, J. Yuan, H. Hu, Q. Yang, J. Li, S. Zhang, et al., The CUL4B/AKT/beta-catenin axis restricts the accumulation of myeloid-derived suppressor cells to prohibit the establishment of a tumor-permissive microenvironment, Cancer Res. 75 (23) (2015) 5070–5083, https://doi.org/10.1158/0008-5472.CAN-15-0898.

[10] Z. Xu, L. Li, Y. Qian, Y. Song, L. Qin, Y. Duan, et al., Upregulation of IL-6 in CUL4B-deficient myeloid-derived suppressive cells increases the aggressiveness of cancer cells, Oncogene 38 (30) (2019) 5860–5872, https://doi.org/10.1038/s41388-019-0847-x.

[11] H. Sung, J. Ferlay, R.L. Siegel, M. Laversanne, I. Soerjomataram, A. Jemal, et al., Global cancer statistics 2020: GLOBOCAN estimates of incidence and mortality worldwide for 36 cancers in 185 countries, CA Cancer J. Clin. 71 (3) (2021) 209–249, https://doi.org/10.3322/caac.21660.

[12] N. Akimoto, T. Ugai, R. Zhong, T. Hamada, K. Fujiyoshi, M. Giannakis, et al., Rising incidence of early-onset colorectal cancer - a call to action, Nat. Rev. Clin. Oncol. 18 (4) (2021) 230–243, https://doi.org/10.1038/s41571-020-00445-1.

[13] L.E. Dow, K.P. O'Rourke, J. Simon, D.F. Tschaharganeh, J.H. van Es, H. Clevers, et al., Apc restoration promotes cellular differentiation and reestablishes crypt homeostasis in colorectal cancer, Cell 161 (7) (2015) 1539–1552, https://doi.org/10.1016/j.cell.2015.05.033.

[14] L.K. Su, K.W. Kinzler, B. Vogelstein, A.C. Preisinger, A.R. Moser, C. Luongo, et al., Multiple intestinal neoplasia caused by a mutation in the murine homolog of the APC gene, Science 256 (5057) (1992) 668–670, https://doi.org/10.1126/science.1350108.

[15] M. Schmitt, F.R. Greten, The inflammatory pathogenesis of colorectal cancer, Nat. Rev. Immunol. 21 (10) (2021) 653–667, https://doi.org/10.1038/s41577-021-00534-x.

[16] T. Jiang, H.M. Tang, Z.H. Wu, J. Chen, S. Lu, C.Z. Zhou, et al., Cullin 4B is a novel prognostic marker that correlates with colon cancer progression and pathogenesis, Med. Oncol. 30 (2) (2013) 534, https://doi.org/10.1007/s12032-013-0534-7.

[17] J.W. Luo, C.M. Wang, J.W. Su, T.Z. Yi, S.H. Tang, CUL4B increases platinum-based drug resistance in colorectal cancer through EMT: a study in its mechanism, J. Cell Mol. Med. 26 (23) (2022) 5767–5778, https://doi.org/10.1111/jcmm.17585.

[18] B. Song, H. Zhan, Q. Bian, J. Li, Knockdown of CUL4B inhibits proliferation and promotes apoptosis of colorectal cancer cells through suppressing the Wnt/beta-catenin signaling pathway, Int. J. Clin. Exp. Pathol. 8 (9) (2015) 10394–10402.

[19] W.B. Su, Z.Y. Liu, MiR-431 inhibits colorectal cancer cell invasion via repressing CUL4B, Eur. Rev. Med. Pharmacol. Sci. 22 (10) (2018) 3047–3052, https://doi.org/10.26355/eurrev_201805_15062.

[20] B. Jiang, W. Zhao, J. Yuan, Y. Qian, W. Sun, Y. Zou, et al., Lack of Cul4b, an E3 ubiquitin ligase component, leads to embryonic lethality and abnormal placental development, PLoS One 7 (5) (2012) e37070, https://doi.org/10.1371/journal.pone.0037070.

[21] S. Huang, Z. Wang, J. Zhou, J. Huang, L. Zhou, J. Luo, et al., EZH2 inhibitor GSK126 suppresses antitumor immunity by driving production of myeloid-derived suppressor cells, Cancer Res. 79 (8) (2019) 2009–2020, https://doi.org/10.1158/0008-5472.CAN-18-2395.

[22] M. Bodogai, K. Moritoh, C. Lee-Chang, C.M. Hollander, C.A. Sherman-Baust, R. P. Wersto, et al., Immunosuppressive and prometastatic functions of myeloid-derived suppressive cells rely upon education from tumor-associated B cells, Cancer Res. 75 (17) (2015) 3456–3465, https://doi.org/10.1158/0008-5472.CAN-14-3077.

[23] C.M. Cattaneo, K.K. Dijkstra, L.F. Fanchi, S. Kelderman, S. Kaing, N. van Rooij, et al., Tumor organoid-T-cell coculture systems, Nat. Protoc. 15 (1) (2020) 15–39, https://doi.org/10.1038/s41596-019-0232-9.

[24] K.K. Dijkstra, C.M. Cattaneo, F. Weeber, M. Chalabi, J. van de Haar, L.F. Fanchi, et al., Generation of tumor-reactive T cells by co-culture of peripheral blood lymphocytes and tumor organoids, Cell 174 (6) (2018) 1586–1598, https://doi.org/10.1016/j.cell.2018.07.009, e12.

[25] M.L. Lennard Richard, D. Brandon, N. Lou, S. Sato, T. Caldwell, T.K. Nowling, et al., Acetylation impacts Fli-1-driven regulation of granulocyte colony stimulating factor, Eur. J. Immunol. 46 (10) (2016) 2322–2332, https://doi.org/10.1002/eji.201646315.

[26] T. Sato, D.E. Stange, M. Ferrante, R.G. Vries, J.H. Van Es, S. Van den Brink, et al., Long-term expansion of epithelial organoids from human colon, adenoma, adenocarcinoma, and Barrett's epithelium, Gastroenterology 141 (5) (2011) 1762–1772, https://doi.org/10.1053/j.gastro.2011.07.050.

[27] T. Sato, R.G. Vries, H.J. Snippert, M. van de Wetering, N. Barker, D.E. Stange, et al., Single Lgr5 stem cells build crypt-villus structures in vitro without a mesenchymal niche, Nature 459 (7244) (2009) 262–265, https://doi.org/10.1038/nature07935.

[28] E. Kadosh, I. Snir-Alkalay, A. Venkatachalam, S. May, A. Lasry, E. Elyada, et al., The gut microbiome switches mutant p53 from tumour-suppressive to oncogenic, Nature 586 (7827) (2020) 133–138, https://doi.org/10.1038/s41586-020-2541-0.

[29] M. Lahde, S. Heino, J. Hogstrom, S. Kaijalainen, A. Anisimov, D. Flanagan, et al., Expression of R-Spondin 1 in Apc(Min/+) mice suppresses growth of intestinal adenomas by altering Wnt and transforming growth factor beta signaling, Gastroenterology 160 (1) (2021) 245–259, https://doi.org/10.1053/j.gastro.2020.09.011.

[30] Y.H. Cho, E.J. Ro, J.S. Yoon, T. Mizutani, D.W. Kang, J.C. Park, et al., 5-FU promotes stemness of colorectal cancer via p53-mediated WNT/beta-catenin pathway activation, Nat. Commun. 11 (1) (2020) 5321, https://doi.org/10.1038/s41467-020-19173-2.

[31] B.K. Koo, D.E. Stange, T. Sato, W. Karthaus, H.F. Farin, M. Huch, et al., Controlled gene expression in primary Lgr5 organoid cultures, Nat. Methods 9 (1) (2011) 81–83, https://doi.org/10.1038/nmeth.1802.

[32] J. Liu, P. Li, L. Wang, M. Li, Z. Ge, L. Noordam, et al., Cancer-associated fibroblasts provide a stromal niche for liver cancer organoids that confers trophic effects and therapy resistance, Cell Mol. Gastroenterol. Hepatol. 11 (2) (2021) 407–431, https://doi.org/10.1016/j.jcmgh.2020.09.003.

[33] Y. Fan, X. Huo, B. Guo, X. Zhang, Y. Yang, J. Lian, et al., Cullin 4b-RING ubiquitin ligase targets IRGM1 to regulate Wnt signaling and intestinal homeostasis, Cell Death. Differ. 29 (9) (2022) 1673–1688, https://doi.org/10.1038/s41418-022-00954-9.

[34] L. Luo, G.Q. Shen, K.A. Stiffler, Q.K. Wang, T.G. Pretlow, T.P. Pretlow, Loss of heterozygosity in human aberrant crypt foci (ACF), a putative precursor of colon cancer, Carcinogenesis 27 (6) (2006) 1153–1159, https://doi.org/10.1093/carcin/bgi354.

[35] A.J. Rowan, H. Lamlum, M. Ilyas, J. Wheeler, J. Straub, A. Papadopoulou, et al., APC mutations in sporadic colorectal tumors: a mutational "hotspot" and interdependence of the "two hits", Proc. Natl. Acad. Sci. USA 97 (7) (2000) 3352–3357, https://doi.org/10.1073/pnas.97.7.3352.

[36] V. Kumar, S. Patel, E. Tcyganov, D.I. Gabrilovich, The Nature of Myeloid-Derived Suppressor Cells in the Tumor Microenvironment, Trends Immunol. 37 (3) (2016) 208–220, https://doi.org/10.1016/j.it.2016.01.004.

[37] E. Mira, R.A. Lacalle, J.M. Buesa, G.G. de Buitrago, S. Jimenez-Baranda, C. Gomez-Mouton, et al., Secreted MMP9 promotes angiogenesis more efficiently than constitutive active MMP9 bound to the tumor cell surface, J. Cell Sci. 117 (Pt 9) (2004) 1847–1857, https://doi.org/10.1242/jcs.01035.

[38] B. Toh, X. Wang, J. Keeble, W.J. Sim, K. Khoo, W.C. Wong, et al., Mesenchymal transition and dissemination of cancer cells is driven by myeloid-derived suppressor cells infiltrating the primary tumor, PLoS Biol. 9 (9) (2011) e1001162, https://doi.org/10.1371/journal.pbio.1001162.

[39] L. Yang, L.M. DeBusk, K. Fukuda, B. Fingleton, B. Green-Jarvis, Y. Shyr, et al., Expansion of myeloid immune suppressor Gr+CD11b+ cells in tumor-bearing host directly promotes tumor angiogenesis, Cancer Cell 6 (4) (2004) 409–421, https://doi.org/10.1016/j.ccr.2004.08.031.

[40] L. Yang, J. Huang, X. Ren, A.E. Gorska, A. Chytil, M. Aakre, et al., Abrogation of TGF beta signaling in mammary carcinomas recruits Gr-1+CD11b+ myeloid cells that promote metastasis, Cancer Cell 13 (1) (2008) 23–35, https://doi.org/10.1016/j.ccr.2007.12.004.

[41] P. Sinha, V.K. Clements, A.M. Fulton, S. Ostrand-Rosenberg, Prostaglandin E2 promotes tumor progression by inducing myeloid-derived suppressor cells, Cancer Res. 67 (9) (2007) 4507–4513, https://doi.org/10.1158/0008-5472.CAN-06-4174.

[42] R. Weber, C. Groth, S. Lasser, I. Arkhypov, V. Petrova, P. Altevogt, et al., IL-6 as a major regulator of MDSC activity and possible target for cancer immunotherapy, Cell Immunol. 359 (2021) 104254, https://doi.org/10.1016/j.cellimm.2020.104254.

[43] P.C. Rodriguez, C.P. Hernandez, D. Quiceno, S.M. Dubinett, J. Zabaleta, J. B. Ochoa, et al., Arginase I in myeloid suppressor cells is induced by COX-2 in lung carcinoma, J. Exp. Med. 202 (7) (2005) 931–939, https://doi.org/10.1084/jem.20050715.

[44] S.K. Bunt, L. Yang, P. Sinha, V.K. Clements, J. Leips, S. Ostrand-Rosenberg, Reduced inflammation in the tumor microenvironment delays the accumulation of myeloid-derived suppressor cells and limits tumor progression, Cancer Res. 67 (20) (2007) 10019–10026, https://doi.org/10.1158/0008-5472.CAN-07-2354.

[45] F. Veglia, M. Perego, D. Gabrilovich, Myeloid-derived suppressor cells coming of age, Nat. Immunol. 19 (2) (2018) 108–119, https://doi.org/10.1038/s41590-017-0022-x.

[46] D. Bayik, J.D. Lathia, Cancer stem cell-immune cell crosstalk in tumour progression, Nat. Rev. Cancer 21 (8) (2021) 526–536, https://doi.org/10.1038/s41568-021-00366-w.

[47] X. Liu, F. Tian, J. Cui, L. Gong, L. Xiang, B. Fan, et al., CUL4B functions as a tumor suppressor in KRAS-driven lung tumors by inhibiting the recruitment of myeloid-derived suppressor cells, Oncogene (2023), https://doi.org/10.1038/s41388-023-02824-1.

[48] M. Ouzounova, E. Lee, R. Piranlioglu, A. El Andaloussi, R. Kolhe, M.F. Demirci, et al., Monocytic and granulocytic myeloid derived suppressor cells differentially regulate spatiotemporal tumour plasticity during metastatic cascade, Nat. Commun. 8 (2017) 14979, https://doi.org/10.1038/ncomms14979.

[49] W. Li, X. Zhang, Y. Chen, Y. Xie, J. Liu, Q. Feng, et al., G-CSF is a key modulator of MDSC and could be a potential therapeutic target in colitis-associated colorectal cancers, Protein Cell 7 (2) (2016) 130–140, https://doi.org/10.1007/s13238-015-0237-2.

[50] G. Kohanbash, K. McKaveney, M. Sakaki, R. Ueda, A.H. Mintz, N. Amankulor, et al., GM-CSF promotes the immunosuppressive activity of glioma-infiltrating myeloid cells through interleukin-4 receptor-alpha, Cancer Res. 73 (21) (2013) 6413–6423, https://doi.org/10.1158/0008-5472.CAN-12-4124.

[51] J.D. Veltman, M.E. Lambers, M. van Nimwegen, R.W. Hendriks, H.C. Hoogsteden, J.G. Aerts, et al., COX-2 inhibition improves immunotherapy and is associated with

decreased numbers of myeloid-derived suppressor cells in mesothelioma. Celecoxib influences MDSC function, BMC Cancer 10 (2010) 464, https://doi.org/10.1186/1471-2407-10-464.

[52] W. Liao, M.J. Overman, A.T. Boutin, X. Shang, D. Zhao, P. Dey, et al., KRAS-IRF2 axis drives immune suppression and immune therapy resistance in colorectal cancer, Cancer Cell 35 (4) (2019) 559–572, https://doi.org/10.1016/j.ccell.2019.02.008, e7.

[53] D. Wang, H. Sun, J. Wei, B. Cen, R.N. DuBois, CXCL1 is critical for premetastatic niche formation and metastasis in colorectal cancer, Cancer Res. 77 (13) (2017) 3655–3665, https://doi.org/10.1158/0008-5472.CAN-16-3199.

[54] W. Lu, W. Yu, J. He, W. Liu, J. Yang, X. Lin, et al., Reprogramming immunosuppressive myeloid cells facilitates immunotherapy for colorectal cancer, EMBO Mol. Med. 13 (1) (2021) e12798, https://doi.org/10.15252/emmm.202012798.

[55] Y. Wang, K. Yin, J. Tian, X. Xia, J. Ma, X. Tang, et al., Granulocytic myeloid-derived suppressor cells promote the stemness of colorectal cancer cells through exosomal S100A9, Adv. Sci. (Weinh) 6 (18) (2019) 1901278, https://doi.org/10.1002/advs.201901278.